DOI: 10.13009/EUCASS2019-485

Compressive response and failure of a micromechanical model for confined unidirectional fiber-reinforced composites

Antonio Settanni and Brina Blinzler** and Alessandro Ceruti****
**University of Bologna*
Via Fontanelle 40, Forlì, Italy - antonio.settanni@studio.unibo.it
***Chalmers University of Technology*
Chalmersplatsen 4, 412 96, Gothenburg, Sweden - brina.blinzler@chalmers.se
****University of Bologna*
Viale Risorgimento 2, Bologna, Italy - alessandro.ceruti@unibo.it

Abstract
The longitudinal compressive response of unidirectional high-stiffness carbon fibres radially confined with glass fibre and embedded in an epoxy matrix are analysed in this study. The method was originally developed for reinforced concrete columns. For this class of hybrid composites, initial fiber misalignment along with material nonlinearity leads to the initiation of fibre kinking. The load carrying capability is expected to be preserved due to the presence of lateral confinement. However, compressive strength is highly depended on fibre alignment. If via manufacturing highly aligned fibres can be formed, then this could potentially lead to micro-buckling failure initiation.

1. Introduction

1.1 Unidirectional composite state-of-the-art

Carbon fibre reinforced polymer (CFRP) materials continue to gain interest in situations where specific stiffness and specific strength are the driving design parameters. Applications such as aeronautical, where fuel consumption is a dominant factor, and space, where payload weight is closely controlled, are two main industries driving innovation in CFRPs. High performance composite materials frequently include layers of unidirectional carbon fibre. While carbon fibre epoxy composites have a high specific tensile strength, the compressive strength is typically 30-40% lower. This comparatively lower axial compression strength typically is observed experimentally in an abrupt failure of unidirectional composites due to fibre instability and kink band formation [1]. This results in composite designs that are frequently limited by the compressive strength. In order to understand how to improve compressive strength via fibre confinement or other means, the micro and meso mechanics of compressive failure must be understood. The exploration of novel confining microstructures via virtual experimentation is an important step in this progress.
A significant amount of research has been conducted in the area of compressive failure analysis of continuous fibre composite materials. Many studies have focused on the damage mechanisms leading to compressive failure, development of modes of compressive failure and interactions between the proposed modes. Initial investigations in compressive failure of unidirectional composites was conducted by Rosen [2] and Argon [3] in the 60s and 70s. Budiansky and Fleck more recent review of compressive failure notes that the dominate failure mode is by plastic kinking [4]. Where high shear loads in the matrix cause plastic deformation of the matrix and the subsequent instability of the unconfined fibre initiates failure. It is clear from this point that a well-defined polymer plasticity model that includes both strain hardening and strain rate effects is required for simulating kink-band formation [4]. Fibre kink-band formation is thought to be a culmination of a number of micromechanics phenomena which act in some unconfirmed order [5, 6, 7, 8, 9, 10]. All current theories include matrix shear crack and/or longitudinal splitting of the matrix among these phenomena leading up to kink-band formation. Matrix shear cracks can form during plastic microbuckling and degrade the matrix around the fibres, reducing matrix confinement and leading to

DOI: 10.13009/EUCASS2019-485

sudden fibre instability [8, 9]. Longitudinal splitting along the interface or in the matrix is a result of the high shear stresses introduced by failure of the nearby plys [7, 10]. Matrix splitting can also be caused by defects introduced in the material during production [10]. Matrix splitting leads to subsequent kink band formation [7, 10]. In general, the development of kink-bands has been determined to be the primary mode of catastrophic failure in unidirectional composites under axial compression loading [4].
The progression of kink band formation is generally too fast to be observed with video [11]. Therefore, the initial damage of the composite and crack progression is difficult to confirm. This has led to a number of modelling approaches that do not consider lateral confinement (apart from the matrix) of the individual fibres and cannot account for alternate kink band formations. Virtual experimentation or modelling is extremely important because it is incredibly difficult to understand this type of damage initiation experimentally. Even with real time imaging of kink band formation, the kink bands propagate too quickly for the initial point to be determined.

1.2 Confinement

Reinforced concrete has found lots of application in the field of construction and building design. Columns of such a structure are able to transfer load and withstand high compressive forces or variable-amplitude loads like earthquakes. Stresses caused by static and dynamic loads may lead to a reduction of the strength of the material or may reduce its ductility [12]. The degradation of material quality may affect the behaviour of the structure bringing on crack initiation and ending up in fatigue failure. Concerning a concrete column, the main object is to guarantee a good dispersive and dissipative behaviour that avoids brittle fracture in the structure and fosters ductile mechanisms. In order to address this issue, adequate ductility is necessary, which is a function of the ability of the materials to undergo high deformations in the elastic range and design considerations that take into account strength and stiffness. It is well known that the most important design parameter that attains an improvement in the ductile response is transverse reinforcement. This is obtained by confining the concrete with spirals, circular or rectangular hoops in order to prevent buckling and shear failure while at the same time increasing both strength and ductility [13]. In particular, all of these effects have an influence also on the flexural strength.
In general, the better the confinement of the core concrete, the higher the bearing capacity to sustain the flexural strength. However, the confinement is also related to the amount of axial compressive load acting on the column which makes the flexural behaviour more dependent on the compressive stress distribution. Also, this distribution is different among the core and the cover concrete and it is reflected by differing confined and unconfined concrete stress-strain relations. This is because only the core concrete carries the stresses at high strains, whereas the cover concrete is inefficient and is represented by the unconfined region. For that reason, it is clear that detailed information concerning stress-strain diagrams are essential to analyze ductility of the columns with different transverse reinforcements.
The main sources of failure of a cement-based column arises due to the compression buckling of the longitudinal bars, fracture of transverse reinforcement, and failure of low cyclic fatigue of longitudinal reinforcement. In order to ensure the enhancement in strength and ductility, different parameters are taken into consideration and the effects on the global behaviour are studied. These variables are: volumetric ratio of lateral steel, spiral spacing, hoop reinforcement and so on [14].
Concerning the effect of volumetric ratio of lateral steel on the confined concrete behaviour, an increment in that parameter results in a increase of strength and ductility, even though the effects on ductility are more apparent than on strength. Generally speaking, the stress-strain curve shows a rapid to moderate decrement in strength beyond the peak. For specimens with a high value of volumetric ratio of spiral reinforcement, lateral steel withstands large values of stresses but longitudinal bars suffer due to buckling phenomena causing the lateral reinforcement to rupture and the column to collapse. In particular, what causes the buckling is the spalling of cover concrete. However, these events occur at large longitudinal strains. Researchers have found the optimal value to be around 1.2 percent.
It has been found that a reduction in spiral spacing determines an increment in both strength and ductility. In most cases, spiral stress at the peak is found to increase whereas, if the maximum stress is close to the yield stress, the confinement effects are not significant. This parameter assumes a very important value to describe confinement behaviour since this controls the buckling of the longitudinal bars [15]. Actually, the tie spacing increases, the confined area decreases and, as a consequence, more premature buckling effects may occur.
Another important outcome concerns the performance and the choice of spiral or circular hoops. At first glance, results prove the same behaviour in both cases. Looking into a more details, hoop reinforced concrete has been found to behave better than spirally reinforced concrete. This is because the rupture of a single hoop does not affect the behaviour of the entire column and does not have any influence on the global confinement effects. On the other hand, the rupture of spirally reinforcement causes the relaxation of the lateral confining stress. As far as the distribution of longitudinal and transverse configuration is concerned, Sheikh proved that, given an even distribution of longitudinal bars, the behaviour is determined by the support lateral ties configuration regardless of its shapes.

Concerning the amount of longitudinal reinforcement, it is considered to not influence the behaviour of the confined cement-based material. There is a strongly likelihood that any difference found in the experimental tests is due to the tests themselves and the stresses in the lateral reinforcement.
For all these reasons, the importance of concrete confined by transverse reinforcement has increasingly attracted more and more researchers. In a recent study, Kim et al. has reported the importance of three other variables, which are the compressive strength of concrete, the yield strength of spiral, and the reinforcement ratio [16]. As far as the compressive strength of concrete is concerned, the confinement enhancement effect is decreased as the concrete compressive strength is increased. This is caused by the limited capacity of concrete for lateral expansion due to the passive confinement of the spirals. Another important conclusion is instead derived about concrete strength and the reinforcement ratio, that is the confinement effect improves as the previous parameters increase.
Despite high-strength concrete presenting a more brittle behaviour compared with normal-strength concrete which requires more lateral confinement, its applicability in buildings has proven a new effective means of confinement without violating the already stringent building code [17]. Hindi, for one, suggested the use of two opposing springs whose spiral spacing can be manipulated to either increase the load carrying characteristics of the column or improve constructability. It has been demonstrated that the use of cross-spiral reinforcement reveals a slight increase in strength and significant improvement in ductility. As a matter of fact, evaluating columns with single spirals and with cross-spiral reinforcement, the average increment in confined compressive strength is set to a percentage of 10.5, assuming the same volumetric confinement ratio. If the volumetric ratio is doubled, strength increases of about 53.7%. In another research of Marvel et al. on the same subject, significant results have been highlighted: a) the maximum core stress and maximum applied load were virtually equal between the conventional spiral and the cross-spiral with twice the spacing using the same amount of confining reinforcement.; b) the ultimate strain and ultimate displacement of the cross-spiral with twice the spacing was on average twenty percent higher than the conventional single spiral; although each had the same amount of confining reinforcement; c) the cross spiral with the same spacing as a conventional single spiral column had significantly higher maximum core stress, maximum applied load, strain capacity and ultimate displacement.
In conclusion, cross-spiral is a promising means of confinement and, in regarding failure of the column, introduces important advantages because spirals rupture at different times.

2. Meso-scale model architecture

The investigation of damage and failure behaviour of the “hybrid” composite has been examined by the finite element (FE) method. The aim of the numerical computation is to provide a comprehensive understanding of the damage phenomena and to explore the efficacy of the modelling techniques. This common methodology for the numerical prediction of stiffness and strength is significant for the large-scale implementation [18]. To capture the internal microstructure, a unit cell model, known also as Representative Volume Element (RVE), composed of fiber tow and matrix, has been developed. This methodology belongs to the class of the multiscale modelling, an efficient method used for the heterogeneous materials such as composite. In this way, the model is separated in three different length scales. Through the adoption of the RVE, the macroscopic mechanical behaviour of a heterogeneous materials is derived. For this reason, the RVE must be the smallest representation of the material, whose model is supposed to be the optimal solution as to reduce the computational cost problem [19]. The 3D architecture model is developed by using the commercial finite element analysis software ABAQUS/CAE.

2.1 Geometry and finite element modelling

The hybrid composite material under study consists of a bundle of high strength/high stiffness unidirectional (UD) fibers wrapped by a confining member and together embedded in a high strength/high modulus resin. The examined micro model is made up of T700S (carbon fibers)/S2 Glass (confinement)/RTM resin. At the initial phase of the modelling framework, it is convenient to make some assumptions. Firstly, a bundle of a hundred UD fibers is chosen to represent the unit cell and the fiber packing is designed at a given volume fraction. Even though a random distribution provides results closer to the experimental data, the fibers are supposed to be evenly distributed around the confining region. Another important assumption is that no filler particle distribution is considered at this first stage. In order to satisfy these conditions, a hexagonal close packing with circular section reinforcement (Figure 1) is chosen to describe the even distribution of the fibers.

DOI: 10.13009/EUCASS2019-485

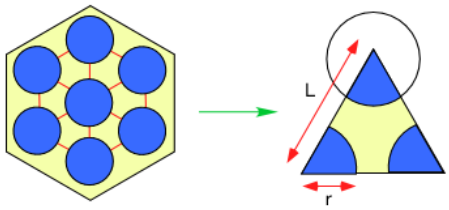

Figure 1: Hexagonal pattern

For a hexagonal array, the fiber volume fraction f is expressed by Equation (1) [20].

$$f = \frac{\text{Area of fibers}}{\text{Area of matrix}} = \frac{3*\frac{\pi r^2}{6}}{\frac{1}{2}L*L*\sin\left(\frac{\pi}{3}\right)} = \frac{2\pi r^2}{\sqrt{3}L^2} \quad \textbf{(1)}$$

Here, r is the radius of the fibers, and L is the distance centre-centre between two fibers. The maximum volume fraction of fibers cannot be higher than 90%, meaning that the fibers are touching. However, 60% is the maximum value that the UD fiber composites can achieve because of the manufacturing process. As a matter of fact, assuming 62% the percentage of fiber volume fraction and 7μm the diameter of the T700S carbon fibers, the distance among fibers is set to 1.5μm.
It is worth noting that, since the initiation of damage due to compressive loads is supposed to occur at the outer row of fibers, the fibers close to the centre, hereinafter called inner fibers, are homogenized handling them as a single homogenized composite material. As far as the reinforcement is concerned, the confinement of the UD reinforced fibers involves the adoption of a helical spring. In particular, a closed and ground ends spring is selected. The adoption of a closed and ground helical compression spring at constant pitch was determined by its capability of creating a radial compression in a very continuous way avoiding peaks. Concerning the bulk matrix, the cubic-shaped model is chosen as to embed the UD fibers and the reinforcement. A change in the mechanical parameters has been observed by changing the size of the micro model. The relevant parameter is the RVE size/fiber size ratio. Particularly, the literature suggests that the correct ratio is RVE/fiber diameter > 8 [19]. The micro model previously obtained satisfies this condition. Hence, the final textile architecture is shown in Figure 2.

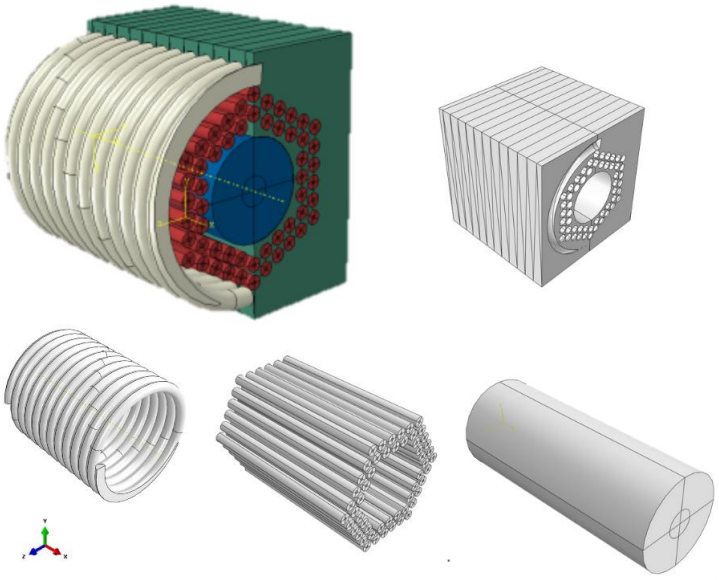

Figure 2: Meso-model consisting of cylindrical fibers, confining spring and matrix

For the finite element discretization, several three-dimensional element types have been assigned to each component. Concerning the inner fiber, linear wedge elements of type C3D6 have been chosen in ABAQUS element library. C3D6 represents a 6-nodes linear triangular prism, reduced integration element. The same element discretization has been preferred for the outer fibers along with linear hexahedral elements of type C3D8R. As far as the reinforcement is concerned, quadratic tetrahedral elements of type C3D10 have been used. Eventually, 10-node quadratic

tetrahedral elements (C3D10H in ABAQUS) have been adopted for the finite element discretization of the matrix. A more detailed representation of the meshed model is reported in Figure 3.

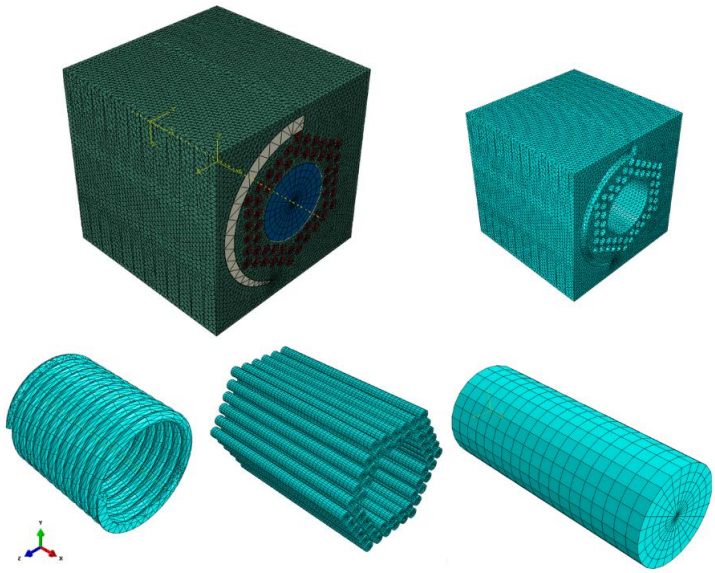

Figure 3: FE meshing of the meso-scale model

To provide the guideline compressive response, the RVE is supposed to have perfect interface between matrix and fibers and matrix and reinforcement. This implies that the master surface corresponding to the matrix is associated with the slave surfaces through tie constraints.
Furthermore, the prescribed boundary conditions are applied to the 3D model. The left bottom corner of the computational model is constrained from all degrees of freedom and a symmetry condition about the axis X is set for the bottom face. On the other hand, a displacement loading is applied on the opposite face and for the right bottom corner movements are allowed around X direction.

2.2 Material constitutive model

The constituent materials are T700S carbon fibers, S2 glass fiber, and 520 RTM resin matrix. TORAYCA T series is characterized by high strength fibers. In particular, T700S has been chosen for the highest tensile strength with standard modulus carbon fibers [21]. AGY's S2 Glass fibers offer more strength compared with traditional glass fibers, high impact resistance, high rigidity, and considerable fatigue resistance [22]. Such enhanced properties deliver better cost performance. Instead, CYCOM PR 520 RTM resin offers superior damage tolerance and good strain to failure for composite primary structure applications [23]. The mechanical properties of the selected materials are listed in Table 1. It is worth noting that since the compressive modulus is unknown for the carbon and glass fibers, the following reasonable assumption is necessary to be defined: tensile modulus is assumed to be equal to compressive modulus.

Table 1: The elastic properties for T700S Carbon, S2 Glass and 520 RTM Matrix

	T700S Carbon	**S2 Glass**	**520 RTM Matrix**
Diameter [μm]	7	9	-
UTS [MPa]	4900	4890	82.1
E_1 [GPa]	230	86.9	4.0
E_2 [GPa]	15	-	-

DOI: 10.13009/EUCASS2019-485

ν_{12}	0.28	0.23	0.398
G_{12} [GPa]	24	-	0.8
G_{23} [GPa]	5.03	-	-

As far as the inner bundle is concerned, the effective properties are obtained [24]. Due to their microscopic heterogeneity, the fiber bundle is modelled as a transversely isotropic UD composite. To fully characterize the behaviour of the homogenized bundle, finite element-based numerical technique, like the RVE homogenization method, has been employed to determine the elastic constants using a hexagonal RVE. The CAE model is depicted in Figure 4.

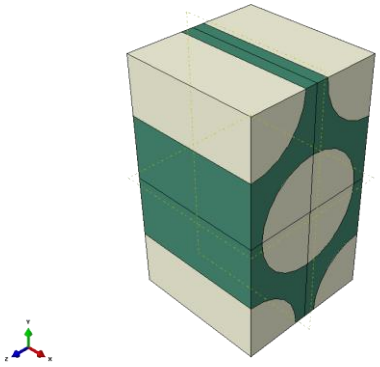

Figure 4: Hexagonal pattern for homogenized inner bundle

To achieve this goal, the imposition of uniform strains on a microscale RVE is required to perform the deformation of the material around the RVE [25]. This means to apply periodic boundary conditions which ensure that the RVE external surfaces still remain periodic. An ABAQUS pug-in, named EasyPBC, comes to the aid of automatically finding and generating the necessary displacement boundary conditions and boundary node sets. For the RVE in Figure 4 (above), modelled in ABAQUS and analyzed using 2750 linear hexahedral elements of type C3D8R and 704 linear wedge elements of type C3D6, the estimated elastic properties are the ones collected in Table 2.

Table 2: Predicted mechanical properties using EasyPBC plug-in

	E_{11} [GPa]	**E_{22} [GPa]**	**E_{33} [GPa]**	**ν_{12}**	**ν_{13}**	**ν_{23}**	**G_{12} [GPa]**	**G_{23} [GPa]**	**G_{13} [GPa]**
T700S/520 RTM	141.88	17.95	17.86	0.32	0.32	0.5	5.63	5.98	5.55

3. Buckling mechanism

Under the ideal manufacturing process, that is highly aligned fibers, micro-buckling failure initiation may occur as failure modes. The term microbuckling is referred to as the deformation of the fibers which behave as columns inside the resin material [26]. Because of the easily visualization and the simple intuition of the process of failure from a physical point of view, it is the most widely studied mode. Researches on this topic have proved that microbuckling is supposed to be influenced by the matrix stiffness in shear, by strain rate, and by environment. Beside this, manufacturing defects, like residual stress, porosity, and fiber misalignment or waviness, affect the deformation of the fibers.

It was Rosen in 1965 the first who investigates the problem in a systematic way. His bi-dimensional model foresees the presence of perfectly straight and evenly spaced fibers, embedded in a linearly elastic matrix [27]. What came to light is the failure in compression by an internal buckling mode. Rosen predicted two possible mode of failure, known as extension mode (or out-of-phase mode) and shear mode (also in-phase mode). The representation of the buckling mode is shown in Figure 5.

DOI: 10.13009/EUCASS2019-485

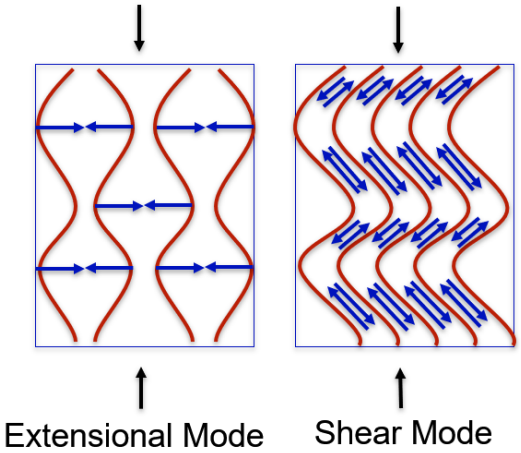

Figure 5: Buckling modes investigated by Rosen

In the former, each fiber deforms π radians out of phase with each other whilst the latter is characterized by adjacent fibers deforming in phase. Rosen deduced the mathematical expressions for the critical buckling stresses in both buckling modes, as presented in Equations (2)-(3).

$$\sigma_{cr} = 2V_f \left[\frac{V_f E_m E_f}{3(1-V_f)}\right]^{\frac{1}{2}} \quad \textbf{(2)}$$

$$\sigma_{cr} = \frac{G_m}{1-V_f} \quad \textbf{(3)}$$

In Equation (2)-(3), σ_{cr} represents the critical compressive strength at buckling, V_f the volume fraction of fibers, E_m and E_f the Young's moduli of matrix and fibers, respectively; G_m the shear modulus of matrix. In addition, Rosen noted that the shear mode occurs assuming that the fibers remain straight unlike the extension mode in which a critical buckle wavelength can be evaluated. The strength of this model is the simplicity of the theory, demonstrated to be very useful to compare the analysis with other models.

3.1 Computational onset of failure

In order to evaluate the critical load of the meso-scale model, an eigenvalue linear elastic buckling analysis is performed [28]. The first step in studying the elastic instability is to determine the critical buckling load and the buckling modes. After the eigenvalue linear analysis, the first three modes of deformation are considered.
At the second step of the analysis, the buckling load factor of the first positive mode of shape is replaced in the load module in ABAQUS and the linear static analysis is performed. The results in terms of stress and displacement are shown in Figure 6-7.

DOI: 10.13009/EUCASS2019-485

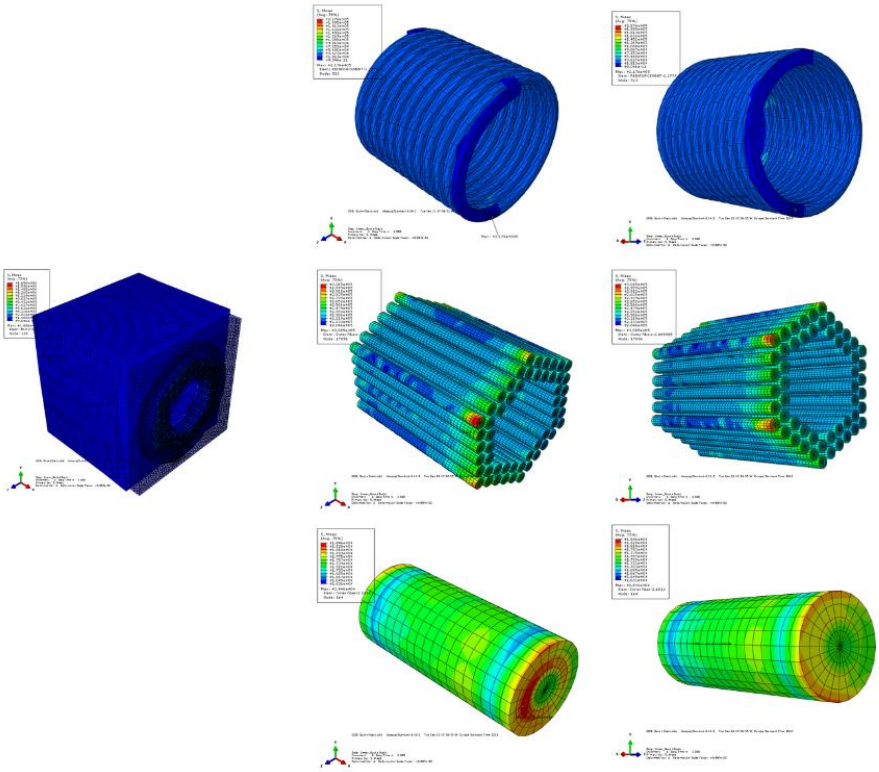

Figure 6: Stress distribution in the whole model and in each component

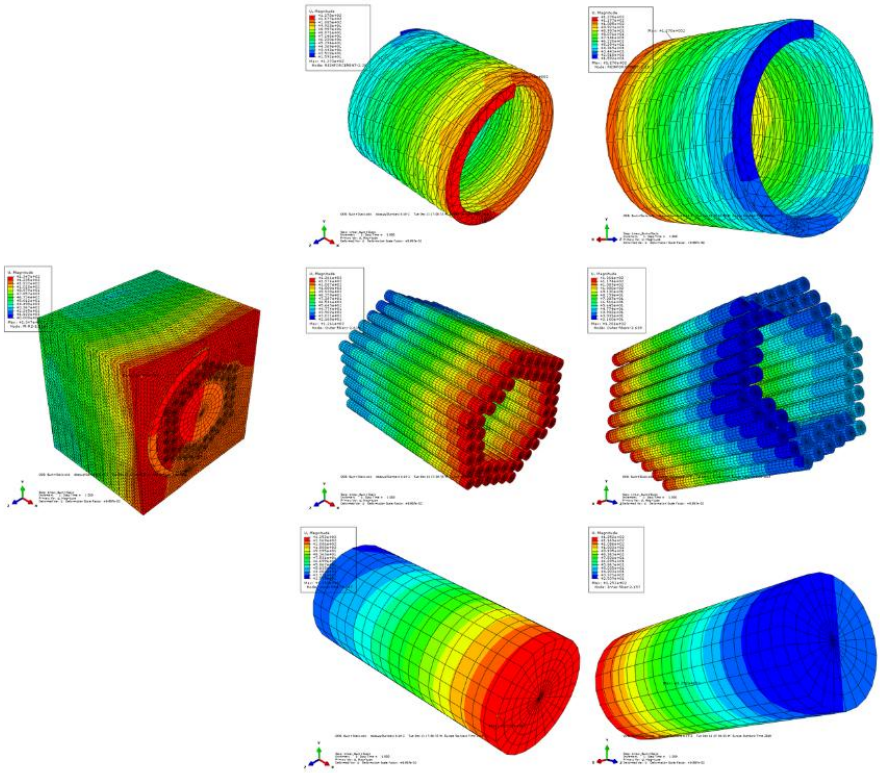

Figure 7: Displacement distribution in the whole model and in each component

3.2 Comparison with analytical theories

In order to ensure the accuracy of the computational model, the results from the previous analysis are compared with the one from Euler's critical buckling theory. The buckling problem is particularly important because it ensures failure will not occur from elastic instability [29]. The fundamental beam buckling problem states that a straight, pin-ended column under compressive load determines a null moment at the end of the column. Under these conditions, the smallest critical load, called Euler's buckling load P_{cr} can be expressed using Equation (4).

$$P_{cr} = \frac{\pi^2 EI}{L^2} \tag{4}$$

The factors affecting the critical load to cause elastic instability are the modulus of elasticity E, the geometric moment of inertia I, the length L and the type of mounting [30]. As far as the Young's modulus is concerned, a stiff material is more resistant to buckle. For this reason, materials with high value of E should be preferred, since strength does not affect buckling phenomenon. Concerning the moment of inertia, the minimum moment of inertia must be used because a column buckles in the direction of minimum resistance. Indeed, the moment of inertia indicates the resistance against deflection. For this reason, the cross-sectional shape has a key role. Usually, hollow sections are more beneficial than solid cross-section. Lastly, the quadratic dependence of the length determines buckling to be one-half the original value.
In addition, in order to determine if the column fails by buckling, Euler's theory allows to calculate the critical buckling stress σ_{cr}. Above this value, the column deforms completely up to the point of total destruction. Equation (5) expresses the buckling stress.

$$\sigma_{cr} = \frac{F}{A} = \frac{\pi^2 E}{\left(\frac{L}{r}\right)^2} \tag{5}$$

Here, A is the cross-sectional area, r is the least radius of the column.
To conclude, the critical load and stress are hand-calculated using Equations (4)-(5) and reported in Table 3. As length of the column, the distance between two adjacent coil of the glass spiral is considered. This distance is equal to 1μm.

Table 3: Critical buckling load and stress using Euler's buckling theory

Buckling load [N]	**Buckling stress [MPa]**
267.6	2.783×10^{10}

4. Kinking mechanism

Kinking is referred to as a localized shear deformation of the matrix in which the fibers are subjected to the fracture at the boundaries of the kink band. It is the matrix stiffness and yield behaviour in shear, and the fiber strength that affect the onset and propagation of kinking. The characterization of the kink band can be described by important parameters, which are the kink band width, the angle of rotation of the fibers, and the angle of the kink band, as shown in Figure 8 [6]. However, the scientific community is still uncertain if considering kinking the final irreversible step of microbuckling or as an independent failure process. As a matter of fact, it was in the late 1977 that Chaplin reported kinking to be an isolated mode of failure, begun from some defects. Regardless the promoting process, kinking is expected to develop along the plane of maximum shear stress or strain in the material. In particular, these planes coincide for a unidirectional composite loaded along the fibers and lie along planes at 45 degrees with respect to the loading axis, even if the material is supposed to be transversely orthotropic. Detailed investigations have revealed that the plane may lie also at angles nearer 60 degrees.
As it is said before, kink band formation is a catastrophic and sudden failure under compressive loads [11]. When a premature event occurs in a local region, such as localized fiber microbuckling or matrix shear, the loads are redistributed locally, leading to excessive loading on the surrounding matrix. In this way, the strain energy is propagated to the undamaged regions, appearing to be a plastically-deformed matrix with broken fibers at the kink boundaries. As a matter of fact, as the load increases and the stress reaches the yield limit, the fibers are subjected to

DOI: 10.13009/EUCASS2019-485

a sliding and a rotation in the area of local limit-load type instability [31, 32]. Large straining occurs inside the kink band whereas relaxation and unloading take place outside the band. However, it is widely acknowledged that the onset of kink band is affected by initial fiber misalignment along with matrix nonlinearity. Argon highlighted the correlation between the mode of failure and the aforementioned parameters.

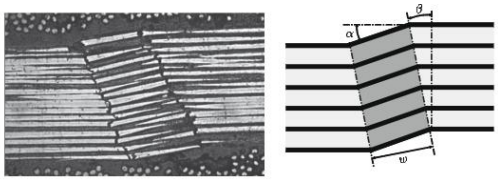

Figure 8: Micrograph of kinking (right) and representation and definition of the parameters (left)

4.1 Modelling overview

A change from the initial version of the model is necessary to take into consideration the geometric imperfection and the nonlinear behaviour of the material. So far considering a uniformly packed three-dimensional model, the geometric imperfection has been introduced through an initial misalignment angle of 1 degree. Instead of tilting the compressive load acting on the top face, the whole model is tilted by a misalignment angle. Figure 9 shows the X-Y plane of the modified RVE.

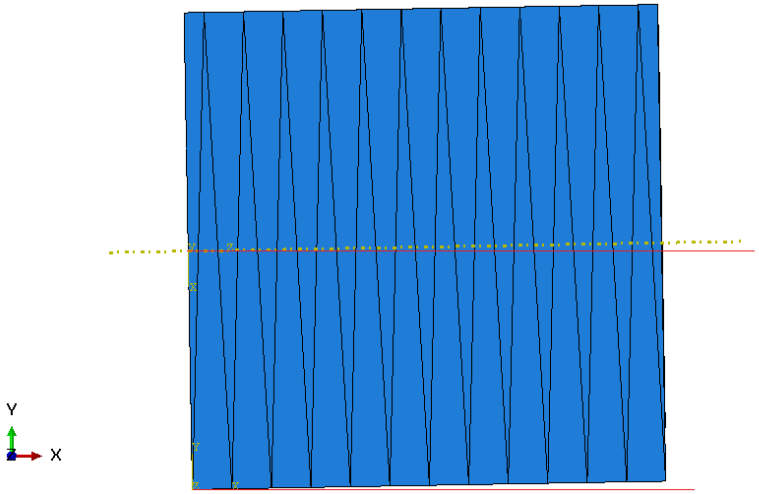

Figure 9: Modified meso-scale model

As far as the material property is concerned, 520 RTM matrix resin is changed with a rubber-toughened epoxy for which the tabular data for plasticity are known. To do this, the PLASTIC material card in ABAQUS allows to introduce the elastic-plastic behaviour of the matrix so as to model the nonlinearity induced in the model due to matrix nonlinearity. The nonlinear compressive stress-compressive strain curve of the bulk rubber-toughened epoxy is shown in Figure 10. The glass fiber is modelled as a linear elastic material whereas the outer carbon fibers are supposed to be orthotropic. Since measuring exactly the orthotropic material properties of the carbon fiber is very difficult, the properties are obtained from different references and tabulated in Table 4.

Table 4: Orthotropic properties of carbon fiber

	E_{11} [GPa]	E_{22} [GPa]	E_{33} [GPa]	ν_{12}	ν_{13}	ν_{23}	G_{12} [GPa]	G_{23} [GPa]	G_{13} [GPa]
T700S	230	15	15	0.28	0.28	0.28	24	5.03	24

DOI: 10.13009/EUCASS2019-485

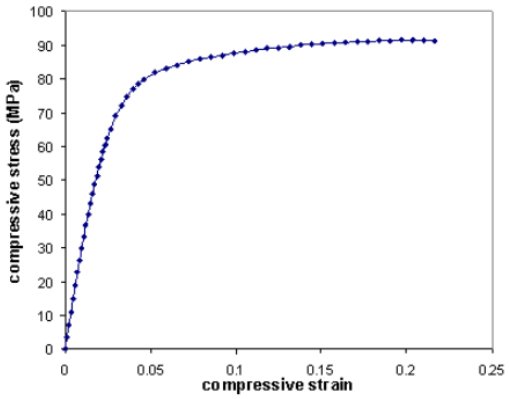

Figure 10: Compressive stress-strain response of the bulk rubber-toughened epoxy

Even though kinking is a dynamic event which involves a large amount of kinetic energy, the problem can be simplified using an arc-length based Riks solver which accommodate the possibility of an unstable snap-back response.

4.2 Nucleation and propagation of kinking

The stress distribution in Figure 11 shows a higher shear stress concentration in the area where the fibers are approximately in contact with the reinforcement. The width of the yield band does not propagate along the other fibers and this is likely related to the presence of the lateral confinement. As a matter of fact, the model does not become unstable and the snap-back behaviour highlighted in other studies [9, 33, 34] is not pointed out.

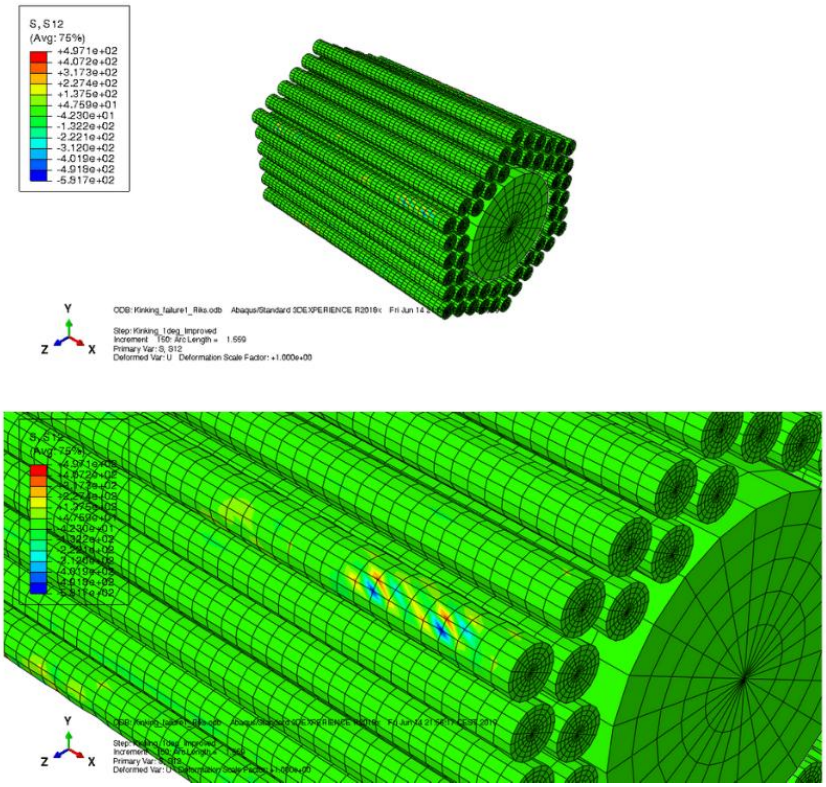

Figure 11: In plane shear stress S_{12}

In Figure 12, the axial stress distribution is reported.

DOI: 10.13009/EUCASS2019-485

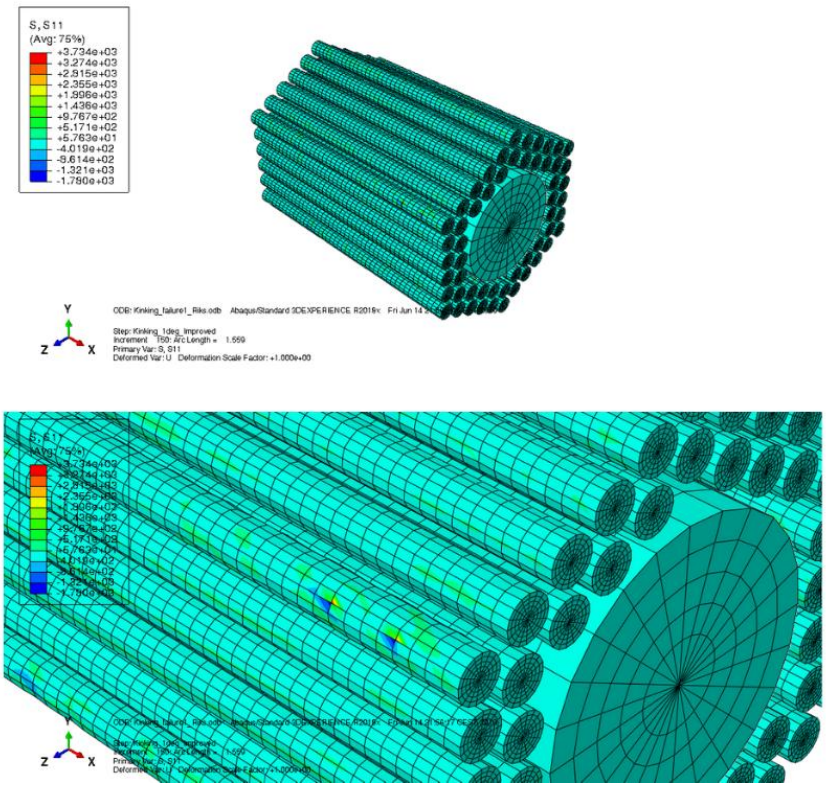

Figure 12: Axial stress distribution S_{11}

5. Results and discussion

The purpose of the buckling and linear static analysis is the determination of the critical load that causes elastic instability for a column. It is worth to recall two different forms of failure that may occur in elastic field, that is buckling and yielding. The latter arises when the stress exceeds the yield strength of the material. The critical buckling stress is usually lower than the yield strength and, as a consequence, the column may buckle before it yields.

First of all, what it is important to notice is the possible mode of failure of the carbon fibers. This issue gives a hint about the development of another failure mechanism, called kinking, which will be addressed further. Looking at the carbon fibers into a more detail, the deformation of the fibers near the zone of maximum stress seems to resemble the shear mode proposed by Rosen. Fibers under examination are shown in Figure 13. It is highly likely that the short length of the fibers will not make the deformation seem like the one suggested by Rosen. For this reason, a further analysis on the length of the fibers is suggested.

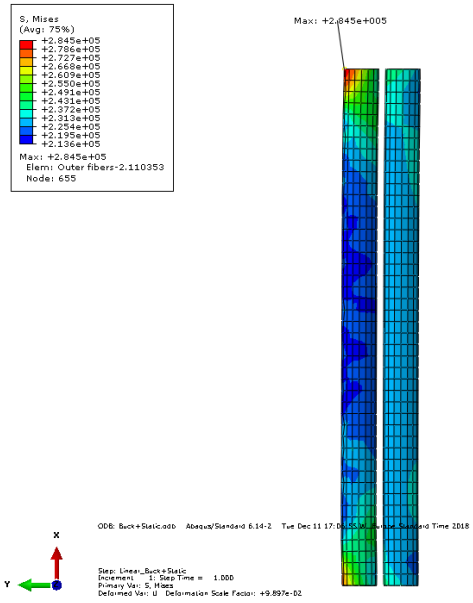

Figure 13: Deformation shape in carbon fibers

Furthermore, to investigate the accuracy of the model representation, the computational results are compared with the numerical solution from the Euler's buckling problem.
As far as the critical buckling load is concerned, the theoretical and computational results are not in good agreement. This may be due to the linear-elastic definition of the materials. Instead, the results concerning the critical stress are arranged in Table 5 and expressed in MPa.

Table 5: Comparison results among different theories

Rosen model	**Euler's buckling theory**	**ABAQUS**
2105	2.783×10^{10}	1.846×10^{10}

The big difference that stands out from Table 5 is the huge variation in the order of magnitude between the Rosen's model and the results from ABAQUS simulation. In effect, the lower value is a consequence of the simplicity of the model proposed by Rosen. As a matter of fact, Rosen neglected lots of terms in the energy balance formulation. On the other hand, the results from Euler's problem and the computational values are in extremely good agreement. In addition, it is the symmetric deformation of the model the main outcome of the analysis, as it is depicted in Figure 7.
As far as kinking is concerned, a distinct difference with other works is deduced. It is widely acknowledged that the onset of kinking in carbon fiber leads to a load drop observed in the stress-strain behaviour. As kinking process continues along the thickness of the model, a transverse failure zone and a slip angle are generated and the fibers in the kink band break. On the other hand, the matrix is at this point subjected to shear stress and starts cracking as the load increases. In the present work, the typical plot in terms of stress-strain is not shown, leading to two main conclusions. Firstly, the model geometry does not facilitate the kinking formation because the initial assumption regarding the number of fibers in the bundle is meagre. Assuming this hypothesis true, it is a geometrical constraint that is insufficient to afford the kink formation. Secondly, the lateral confinement produces an outstanding contribution. The fibers are meant to be locked inside the confinement region and the kink band are expected to be risen. Although the characterization of the model in such a way brings to primary important results, future works are recommended with respect to a better definition of the plasticity model and the modelling of the interface between each component of the RVE.

DOI: 10.13009/EUCASS2019-485

6. Conclusions

The development of a 3D FE based micromechanical model is carried out in a computational way since the compressive loading makes it difficult to understand the nucleation and propagation of two of the main phenomenon which develop inside the material. Although there are parameters that are neglected in this preliminary study like the interface properties, the randomness of the unidirectional carbon fibers, and the manufacturing process associated defects, the micro-model has given a better estimation of the initial processes of damage and failure. As a matter of fact, a detailed micromechanical modelling of the RVE is undertaken to account for the periodicity of the fibers architecture. In this way, a microscale FE model provides a powerful tool to study the composite mechanical response and to describe the progressive damage initiation.
Under the assumption of highly aligned fibers, fiber micro-buckling is studied employing a buckle and linear static solver. The prediction of the critical buckling stress has been compared qualitatively with the one obtained using Euler's Theory of Column. The results from both the analytical and computational model prediction have shown a good agreement.
Subsequently, initial fiber misalignment along with material nonlinearity have been introduced into the model to investigate the initiation of a fiber kinking mechanism. A better understanding of the mechanisms of failure is meaningful to improve the compressive performance of the material. However, future works are strongly recommended in order to extract the compressive strength limiting mechanism of such a new material that have the appearance to be very promising.

References

[1] Soutis, C. 1997. Compressive Behaviour of Composites. Rapra Technology Limited.
[2] Rosen, V.W. 1965. Mechanics of Composite Strengthening: Fibre Composite Materials. In *American Society of Materials: Metals Park*. Chapter 3.
[3] Argon, A.S. 1972. Fracture of Composites. *Treatise on Materials Science and Technology*. 1:79-114.
[4] Budiansky, B. and Fleck, N.A. 1993. Compressive failure of fibre composites. *Journal of the Mechanics and Physics of Solids*. 41:183-211.
[5] Vogler, T.J. and Kyriakides, S. 2001. On the initiation and growth of kink bands in fiber composites: Part I. Experiments. *International J. of Solids and Structures*. 38(15):2639-2651.
[6] Pimenta, S., R. Gutkin, S.T. Pinho, and P. Robinson. 2009. A micromechanical model for kink-band formation: Part I – Experimental study and numerical modelling. *Composites Science and Technology*, 69(7-8):948-955.
[7] Hapke, J., F. Gehrig, N. Huber, K. Schulte, and E.T. Lilleodden. 2011. Compressive failure of UD-CFRP containing void defects: In situ SEM microanalysis. *Composites Science and Technology*. 71(9):1242-1249.
[8] Lee, S.H., and Waas, A.M.. 1999. Compressive response and failure of fiber reinforced unidirectional composites. *International Journal of Fracture*. 100:275-306.
[9] Patel, D.K., A.M. Waas, and C. Yen. 2019. Compressive response of hybrid 3D woven textile composites (H3DWTCs): An experimentally validated computational model. *Journal of the Mechanics and Physics of Solids*. 122:381-405.
[10] Pinho, S.T., R. Darvizeh, P. Robinson, C. Schuecker, and P.P. Camanho. 2012. Material and structural response of polymer-matrix fibre-reinforced composites. *Journal of Composite Materials*. 46(19-20):2313-2341.
[11] Wang, Y., Y. Chai, C. Soutis, and P.J. Withers. 2019. Evolution of kink bands in a notched unidirectional carbon fibre-epoxy composite under four-point bending. *Composites Science and Technology*. 172:143-152.
[12] El-Kholy, A.M., and H. A. Dahish. 2016. Improved confinement of reinforced concrete columns. *Ain Shams Engineering Journal*. 7(2):717-728.
[13] Mander, J.B., M.J.N. Priestley, and R. Park. 1988. Theoretical stress-strain model for confined concrete. *J. Struct. Eng*. 114(8):1804-1826.
[14] Shamim, A., and M.T. Toklucu. 1993. Reinforced concrete columns confined by circular spirals and hoops. *ACI Structural Journal*. 90:542-553.
[15] Sheikh, S.A., and S.M. Uzumeri. 1980. Strength and ductility of tied concrete columns. *Journal of the Structural Division*. 106(5):1079-1102.
[16] Kim S., Y. Kim, J. Lee, and K. Kim. 2017. Confined concrete with varying yield strengths of spirals. *Magazine of Concrete Research*. 69(5):217-229.
[17] Marvel, L., N. Doty, W. Lindquist, and R. Hindi. 2014. Axial behavior of high-strength concrete confined with multiple spirals. *Engineering Structures*. 60:68-80.

[18] Zhang, D., A.M. Waas, and C. Yen. 2015. Progressive damage and failure response of hybrid 3D textile composites subjected to flexural loading, part II: Mechanics based multiscale computational modelling of progressive damage and failure. *International Journal of Solid and Structures*. 75-76:321-335.
[19] Riano, L., L. Belec, and Y. Joliff. 2016. Validation of a Representative Volume Element for unidirectional fiber-reinforced composites: Case of a monotonic traction in its cross section. *Composite Structures*. 154:11-16.
[20] Vasiliev, V.V., and E.V. Morozov. 2018. Advanced Mechanics of Composite Materials and Structures. Elsevier.
[21] Toraya Composite Materials America, Inc. *Types of carbon fiber*. https://www.toraycma.com/page.php?id=661.
[22] AGY. 2006. High strength glass fibers. Pub. No. LIT-2006-111 R2 (02/06)
[23] Cytec. Engineered Materials. 2012. Cycom PR 520 RTM Resin System. AECM-00012. REV:01.
[24] Zhang, C., W.K. Binienda, R.K. Goldber, and L.W. Kohlman. 2014. Meso-scale failure modeling of single layer triaxial braided composite using finite element method. *Composite Part A Applied Science and Manufacturing*. 58:36-46.
[25] Omairey, S., P.D. Dunning, and S. Sriramula. 2018. Development of an ABAQUS plugin tool for periodic RVE homogenisation. *Engineering with Computers*. 35(2):567-577.
[26] Schultheisa, C., and A.M. Waas. 1996. Compressive failure of composite, Part I: Testing and micromechanical theories. *Progress in Aerospace Sciences*. 32(1):1-42.
[27] Argon, A.S. 1972. Fracture of composite. *Treatise on Materials Science and Technology*. 1:79-114.
[28] ABAQUS/CAE User's Manual.
[29] Beeman, A. 2014. Column Buckling Analysis. Engineering project. Rensselaer Polythechnic Institute, Faculty of Rensselaer Polytechnic Institute.
[30] Cacho-Perez, M., A. Lorenzana, P.M. Lopez-Reyes, and R. Saiz. 2010. Method to determine in a simple way the critical load, considers possibility of variable cross-section under any type of load (including thermal loading). In: *Conference: IV European Conference on Computational Mechanics. Solid, Structures and Coupled Problems in Engineering*. 1-10.
[31] Prabhakar, P., and A.M. Waas. 2013. Interaction between kinking and splitting in the compressive failure of unidirectional fiber reinforced laminated composites. *Composite Structures*. 98:85-92.
[32] Bishara, M., R. Rolfes, and O. Allix. 2017. Revealing complex aspects of compressive failure of polymer composites – Part I: Fiber kinking at microscale. *Composite Structures*. 169:105-115.
[33] Jensen, A.B., J. Thesbjerg, J.L. Wind, and H.M. Jensen. 2019. Kink band predictions in fiber composites using periodic boundary conditions. *Composite Structures*. 207:331-339.
[34] Pimenta, S., R. Gutkin, S.T. Pinho, and P. Robinson. 2009. A micromechanical model for kink-band formation: Part II – Analytical modelling. *Composites Science and Technology*. 69:956-964.